Hindawi
International Journal of Antennas and Propagation
Volume 2019, Article ID 5937973, 12 pages
https://doi.org/10.1155/2019/5937973

Research Article

Theoretical and Experimental Study on Echo Fluctuation Suppression of a Cirrus Cloud by Millimeter Wave MIMO Radar

Jinhu Wang,[1,2,3,4] **Junxiang Ge**,[2] **Ming Wei**,[1] **Hongbin Chen**,[4] **Zexin Yang**,[2] **Yushu Ren**,[1] **Qilin Zhang**,[1] **and Hao Chen**[1]

[1]*Collaborative Innovation Center on Forecast and Evaluation of Meteorological Disasters, Key Laboratory for Aerosol-Cloud-Precipitation of China Meteorological Administration, Nanjing University of Information Science and Technology, Nanjing 210044, China*
[2]*Jiangsu Key Laboratory of Meteorological Observation and Information Processing, Nanjing University of Information Science and Technology, Nanjing 210044, China*
[3]*National Demonstration Center for Experimental Atmospheric Science and Environmental Meteorology Education, Nanjing University of Information Science and Technology, Nanjing 210044, China*
[4]*Key Laboratory of Middle Atmosphere and Global Environment Observation, Institute of Atmospheric Physics, Chinese Academy of Sciences, Beijing 100029, China*

Correspondence should be addressed to Jinhu Wang; goldtigerwang@nuist.edu.cn

Received 18 April 2018; Revised 25 August 2018; Accepted 27 September 2018; Published 13 January 2019

Academic Editor: Lorenzo Luini

The scattering properties of nonspherical particles can be approximately computed by equivalent spherical theory. The scattering properties of ice particles were approximately computed by Rayleigh approximation because the sizes of the ice particles are smaller than the wavelength of millimeter wave radar. Based on the above assumption, the echo fluctuation of moving particles was analyzed by computing the total backscattering field of a cirrus cloud using the classical vector potential technique. The simulation results showed that echo fluctuation influences the accuracy of retrieving the physical parameters of a cloud. To suppress the echo fluctuation of moving ice particles, a video integrator of a millimeter wave cloud radar would be used. However, video integrators lose the rapidly changing information of ice particles and reduce radar range resolution; thus, we propose the pace-diversity technique of MIMO radar to reduce the echo fluctuation, which could be validated by theoretical computation and experimental measurements.

1. Introduction

Cirrus clouds are globally distributed and play an important role in regulating the energy budget in the earth-atmosphere system, but they are still a source of major uncertainties in satellite and climate modeling studies [1–5].

To study macro- and microphysical properties such as cloud height, cloud thickness, and ice water content (IWC), active and passive remote sensing instruments that cover visible, infrared, and millimeter and submillimeter wavelengths have been adopted. These instruments include satellite instruments, such as TRMM (tropical rainfall measuring mission) [6] and CloudSat [7]; airborne-based instruments, such as WCR (U. of Wyoming) [8] and ACR (UMass and NASA) [9]; and ground-based instruments, such as MMCR (ARM millimeter wave cloud radar) [10] and CPRS (cloud profiling radar system) [11]. Among them, millimeter wavelength radars have an advantage in detecting the dynamic and structural properties of cirrus clouds [12]. To retrieve the physical properties of clouds, the interaction between electromagnetic waves and ice particles should be studied.

Before studying the scattering properties, the size and shape of cirrus clouds have to be confirmed. Cirrus clouds are composed of almost nonspherical ice crystals with various sizes and shapes. Some numerical methods have been widely used to calculate the scattering properties of cirrus

cloud particles, such as the T-matrix [13], the finite difference time domain (FDTD) [14], the discrete dipole approximation (DDA) [15], the finite element method (FEM) [16], and the method of moments (MOM) [17]. However, these ice particles are smaller compared to the wavelength of a millimeter wave and are usually randomly orientated, so the scattering properties of an ice cloud can be approximately calculated by the Rayleigh approximation [18].

At present, few researchers discuss the characteristics of a scattering electromagnetic wave when ice particles are in motion because modern weather radar has been equipped with video integrators, which can obtain the average value of received power by integral calculation [19]. Video integrators can transform the video signal, which can amplify the video signal and conduct analog-to-digital conversion and integration processing. Integration processing consists of calculating the distance integral and azimuth integral. However, video integrators have the disadvantage of reducing the distance resolution and have high average time requirements [20]. The radial resolution Δr of radar has the following relationship with the pulse width τ and velocity of light C: $\Delta r = (1/2) * \tau * C$. If we use a video integrator, then the integrated times of distance K would be introduced, with which the radial resolution Δr of radar has the following relationship along with the pulse width τ and velocity of light C: $\Delta r = (1/2) * K * \tau * C$. When the pulse width τ remains unchanged, the video integrator would reduce the resolution Δr of the radar range due to K.

These factors led to an important question: how can we suppress echo fluctuation (RCS fluctuation) without reducing the distance resolution? To solve this problem, first, the echo fluctuation phenomenon of the moving spherical particles was simulated by using the vector potential method under the Rayleigh approximation. Second, we studied the reason why video integrators would reduce the resolution of the radar range and easily lose changed information and we suggested that the best way to suppress echo fluctuation is MIMO radar. To validate the suppression effect of MIMO radar, the RCS values of horizontally orientated hexagonal columns, ellipsoids, and spherical particles were simulated theoretically by HFSS software and compared with the results of detecting moving particles with vertically pointing radar. To experimentally validate the echo fluctuation suppression ability of MIMO radar, the RCS values of cuboid candles based on MIMO spatial diversity were measured in a microwave anechoic chamber at Nanjing University of Information Science and Technology.

2. Analysis of Echo Fluctuation

When the radar transmitter transmits an electromagnetic pulse, an accurate timer is started to measure the time between the starting transmitting pulse and the received echo signal, which is scattered by atmospheric particles. The distance between the radar and the atmospheric particle can be deduced from the consumed time and the speed of light. The atmospheric particles are randomly distributed in space. The magnitude and phase of the electromagnetic waves scattered by atmospheric particles are randomly changed with the enhancement and attenuation of the interference. Atmospheric particles are not fixed at a certain position: assuming the amplitude of the electromagnetic wave scattered to the radar is A, the fluctuating distribution follows the Rayleigh probability distribution, which leads to probability distributions of backscattered power in the forms of A^2, and then, average processing would be used in order to retrieve the parameters of particles, which are proportional to the backscattering cross section of all particles in the unit volume [21].

To analyze the echo fluctuation of moving ice particles, the scattering properties of moving ice particles must first be computed. Mie theory [22] can be used to compute the scattering properties of ice particles because an ice cloud can be made of approximately spherical particles. Logan has reviewed the early history of light scattering [23], and the book written by Stratton has outlined this theory in terms of spherical vector wave functions. Professor Shanjie Zhang discussed the plane electromagnetic wave scattering of spherical particles using vector potential [24]. Rayleigh approximation is a special case of Mie scattering that describes the elastic scattering of light by spherical particles, which is much smaller than the wavelength of incident electromagnetic waves [25]. The monographs written by Van de Hulst and Bohren and Huffman have provided a concrete derivation [26, 27]. The vector potential technique was used, and the phenomenon of echo fluctuation produced by moving particles is studied in this paper. Because the ensembles of ice particles are sparse, the mutual interaction would not be considered.

According to Maxwell equations in a linear, isotropic, homogeneous medium, the charge density and current density are $\rho = 0$ and $\overrightarrow{J} = 0$, respectively, and the time-harmonic electromagnetic fields $(\overrightarrow{E}, \overrightarrow{H})$ will satisfy the wave equation; thus, the scattering electric field intensity of the spherical particles in the spherical coordinate system can be obtained by the vector potential technique [24]:

$$\begin{cases} E_r^s = 0, \\ E_\theta^s = \dfrac{E_0 \cos\phi}{(k_0 r)^3} (k_0 a)^3 \dfrac{\varepsilon_r - 1}{\varepsilon_r + 2} - j \dfrac{E_0 \cos\phi}{(k_0 r)^2} (k_0 a)^3 \dfrac{\mu_r - 1}{\mu_r + 2}, \\ E_\phi^s = \dfrac{E_0 \sin\phi}{(k_0 r)^3} (k_0 a)^3 \dfrac{\varepsilon_r - 1}{\varepsilon_r + 2} - j \dfrac{E_0 \sin\phi}{(k_0 r)^2} (k_0 a)^3 \dfrac{\mu_r - 1}{\mu_r + 2}, \end{cases} \tag{1}$$

where E_0 is the amplitude of an incident electromagnetic wave, $k_0 = \omega\sqrt{\varepsilon_0 \mu_0}$ is the wave number of the incident electromagnetic wave, ε_0 and μ_0 are the dielectric constant and magnetic permeability (usually air) outside the sphere, respectively, r is the distance between the center of sphere and the scattering observation point, a is the radius of the spherical particle, ϕ is the azimuth angle in the spherical coordinate system, and ε_r and μ_r are the relative permittivity and permeability of the spherical particles, respectively.

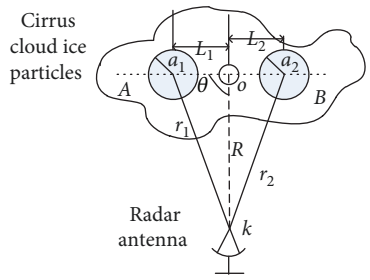

Figure 1: The geometric relationship between two particles and radar antenna.

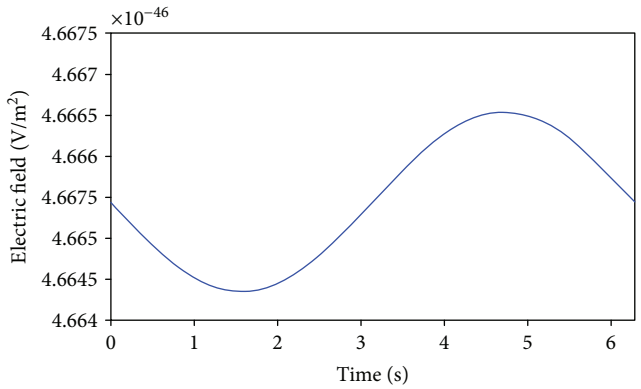

Figure 2: Variations in received electric field as a function of time when spherical particles move at the angular velocity of 1 rad/s.

Whether they are "E-plane" or "H-plane," the total scattering electromagnetic field can be expressed as follows:

$$\begin{aligned} \left|E_{\text{total}}^{\text{sca}}\right|^2 &= \left|E_r^{\text{sca}}\right|^2 + \left|E_\theta^{\text{sca}}\right|^2 + \left|E_\phi^{\text{sca}}\right|^2 \\ &= \left(\frac{E_0 a^3}{r^3}\frac{\varepsilon_r - 1}{\varepsilon_r + 2}\right)^2 + \left(\frac{E_0 a^3 k_0}{r^2}\frac{\mu_r - 1}{\mu_r + 2}\right)^2. \end{aligned} \quad (2)$$

The received radar power P_r is proportional to the scattering electromagnetic fields $\left|E_{\text{total}}^{\text{sca}}\right|^2$ or $\left|H_{\text{total}}^{\text{sca}}\right|^2$, and P_r can be obtained by $\left|E_{\text{total}}^{\text{sca}}\right|^2$ [19]. To compute more conveniently, taking two rotating particles as an example and assuming an incident electromagnetic field is $E_0 = 10$ kV/m, the frequency of the millimeter wave radar is 94 GHz, and the equivalent dielectric constant of the particle is $\varepsilon = 3.1307 - j0.0111$ [28]. The radii of spherical particles A and B are 10 μm and 8 μm, respectively, the distance between A and B is 0.8 m, and the distance between the radar antenna and the center of the ensembles of ice particles is 6000 m, which can be found in Figure 1.

Assuming the two particles are spatially rotated clockwise at angular velocity ($\Omega(t) = 1$ rad/s) under the wind vector gradient, the starting position can be as shown in Figure 1, the change in distance between the radar antenna and the particles can be computed at 0 to 6.28 seconds, and the received electric field as a function of time can be found as shown in Figure 2 using equation (2).

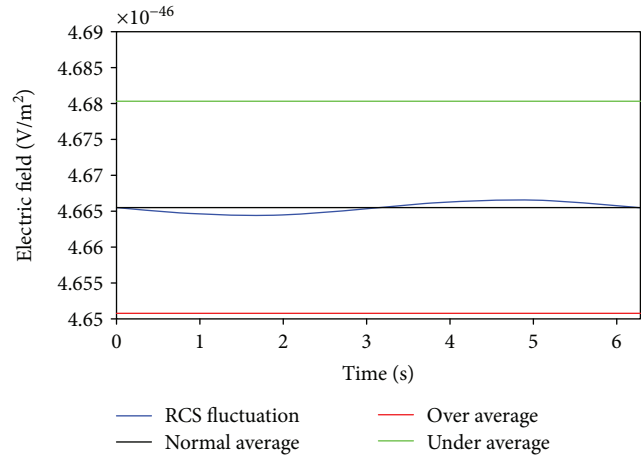

Figure 3: Simulation results of echo fluctuation under three average methods.

Figure 2 shows the electric field received at the radar antenna along with changes in time in the situation of a cosine function when the particles move at an angular velocity of 1 rad/s; the changed received electric field makes it impossible to accurately obtain the received power, and the physical parameters of the cloud cannot be accurately retrieved based on this power. The reason cosine function fluctuates is that the distance between the spherical particles and the radar antenna depends on the cosine of the angle θ in Figure 1. To reduce the influence of RCS fluctuation on the retrieval of cloud physical parameters, the weather radar uses the video integrator to suppress the echo fluctuation. However, if the average time is not sufficient, the measured average power still fluctuates greatly; if the average time is too long, the actual change characteristic of the ice particles will be smoothed out and lose their original information. It should be noted that the video integrator can not only suppress echo fluctuation but also reduce the distance resolution [20].

3. Echo Fluctuation Suppression by Single Millimeter Wave Radar

At present, the single radar uses the video integrator to suppress the echo fluctuation of the moving particles, using average technology to suppress the echo fluctuation as shown in Figure 2. Assume that the radar collects 128 points in 6.28 seconds and define three average numbers: (1) normal average, the average number of times is 128; (2) over average, the average number of times is 130; and (3) under average, the average number of times is 126. The simulation results of echo fluctuation under above three average methods can be found in Figure 3.

Figure 3 shows that the results of echo fluctuation suppression using the normal average are the best. The results of echo fluctuation suppression using the over average are lower, and those with the under average are higher than the actual values (RCS fluctuation), which are results consistent with the conclusions of the video integrator in radar meteorology [19].

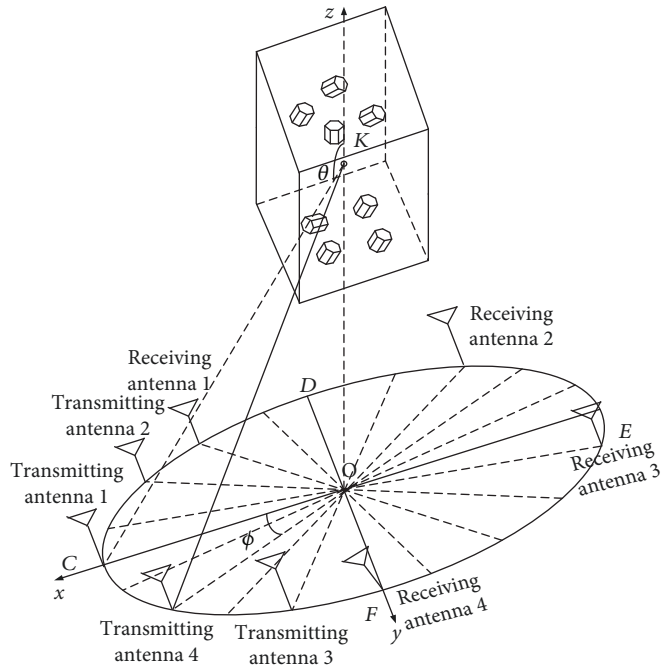

Figure 4: A schematic of a cirrus cloud detected by round MIMO array.

Table 1: Parameter settings of the transmitting antennas in HFSS software.

Number	Definition of E	Definition of K
T1	SP (0,0,0); TP(0,−1,0)	SP (0,0,0); TP(−2000,0,600)
T2	SP (0,0,0); TP(1175.6,1618,0)	SP (0,0,0); TP(−1618,1175.6,6000)
T3	SP (0,0,0); TP(1902.1,−618.034,0)	SP (0,0,0); TP(−618.034,−1902.1,6000)
T4	SP (0,0,0); TP(1175.6,−1618,0)	SP (0,0,0); TP(−1618,−1175.6,6000)

T stands for transmitting antenna, SP stands for starting point, TP stands for terminal point, E stands for electric filed, and K stands for the propagation direction of the electromagnetic wave.

In summary, the conventional video integrator of meteorological radar can suppress the echo fluctuation with the situation of a normal average. However, a video integrator will reduce the radar range resolution, and under- and oversuppression phenomena easily appeared when the average number of times was lesser or greater than the normal average, respectively. In addition, the video integrator would reduce the radar range resolution. Therefore, it is of great significance to explore the millimeter wave MIMO radar to suppress the echo fluctuation of moving particles.

4. Echo Fluctuation Suppression Theory and Experiment by MIMO

4.1. MIMO Simulation of Echo Fluctuation Suppression. To verify the echo fluctuation suppression ability of MIMO radar, it is assumed that a nonspherical ice particle is a hexagonal column, which is one of the most common particles in cirrus clouds [29]. A theoretical simulation of echo fluctuation suppression using a $4 * 4$ MIMO antenna array can be found in Figure 4.

Table 2: Parameter settings of receiving antennas in HFSS software.

Number	Azimuth angle	Pitch angle
R1	90°	161.5651°
R2	162°	161.5651°
R3	234°	161.5651°
R4	306°	161.5651°

R stands for receiving antenna.

In Figure 4, the diameter of the circular array is 4000 m, the distance between the center O of the circular array and the center K of the cloud particles is 6000 m, OC is the positive direction of x, OF is the positive direction of y, and OK is the positive direction of z. The parameters of the transmitting antennas and receiving antennas set in HFSS (high-frequency structure simulator) software can be found in Tables 1 and 2, respectively.

We assume that the targets detected by the MIMO radar array in Figure 4 are ensembles of hexagonal columns, long ellipsoid particles, and spherical particles, which have the same volume. The complex refraction indices of these particles

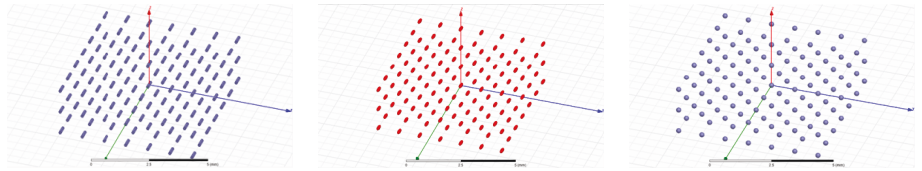

(a) (b) (c)

Figure 5: Ensembles of (a) hexagonal columns, (b) ellipsoids, and (c) spheres simulated by HFSS software.

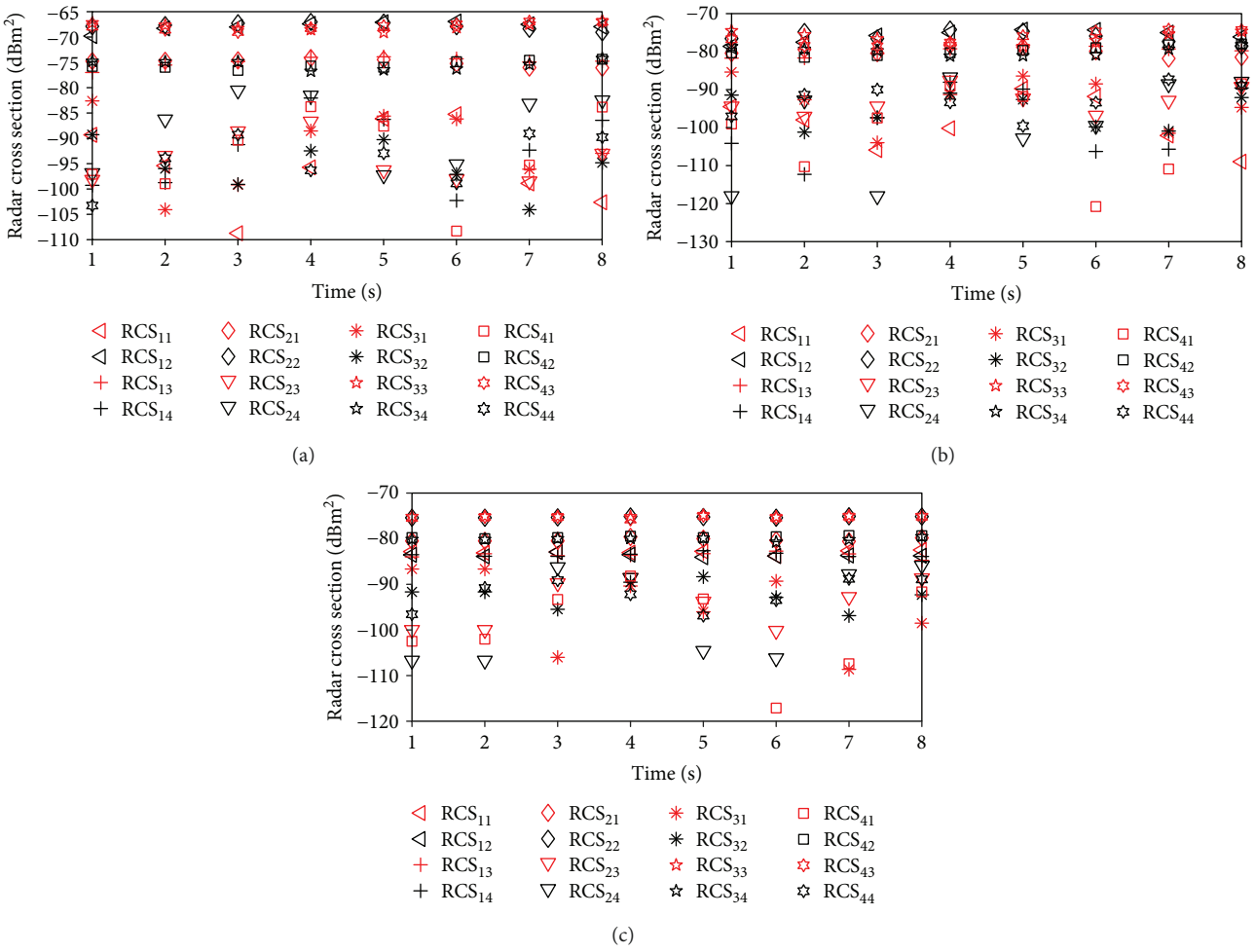

Figure 6: RCS simulation results of horizontally orientated (a) hexagonal columns, (b) ellipsoids, and (c) spheres by means of MIMO.

are $m = 1.782 + j * 0.0027$, and the corresponding complex permittivities are $\varepsilon = 3.1755 + j * 0.0096$ [30]. The long side and short side of the hexagonal column are 400 μm and 69.6000 μm, respectively; the axis of the long half of the ellipsoid is 200 μm, and the axis of the short half is 77.5186 μm. The radius of the spherical particle is 106.3197 μm, and the volumes of the three particles are $5.0342 * 10^6$ μm. The simulated models of ensembles of ice particles in the HFSS environment can be found in Figure 5.

The arrangements of ensembles of hexagonal columns, ellipsoids, and spherical particles are shown in Figures 5(a)–5(c), respectively. These models of particles consist of 147 identical particles. These particles are arranged in the upper and lower left and right spaces with the distance of 1 mm. The definitions of transmitting antenna and receiving antenna of MIMO radar are shown in Tables 1 and 2, respectively, and the incident electromagnetic wave frequency is 94 GHz. The positions of rotated ensembles of particles at 1 s are shown in Figure 5. The positions of rotated ensembles of particles at 2 s, 3 s, 4 s, 5 s, 6 s, 7 s, and 8 s are rotated counterclockwise by 20°, 40°, 60°, 80°, 100°, 120°, and 140°, with Figure 5 chosen as a benchmark. The simulated RCS values of ensembles of hexagonal columns, ellipsoids, and spherical particles can be found in Figure 6.

Figures 6(a)–6(c) show RCS simulation results of horizontally orientated hexagonal columns, ellipsoids, and spheres,

Table 3: The difference between the maximum and minimum RCS fluctuation by means of MIMO (units: dB).

Number	Horizontally orientated hexagonal columns	Horizontally orientated ellipsoids	Horizontally orientated spheres
T1 + R1	23.48	19.21	1.29
T1 + R2	2.88	4.37	1.139
T1 + R3	3.09	3.44	2.029
T1 + R4	20.22	24.26	1.27
T2 + R1	1.91	3.56	0.95
T2 + R2	2.05	4.34	0.31
T2 + R3	11.81	9.51	11.59
T2 + R4	16.74	31.29	20.82
T3 + R1	21.47	18.59	21.99
T3 + R2	14.80	10.27	8.54
T3 + R3	2.26	4.15	0.36
T3 + R4	2.51	2.99	1.19
T4 + R1	24.55	32.32	28.92
T4 + R2	2.20	3.50	0.67
T4 + R3	2.05	4.38	0.82
T4 + R4	14.21	12.29	8.06

T stands for transmitting antenna, R stands for receiving antenna, and + stands for combination.

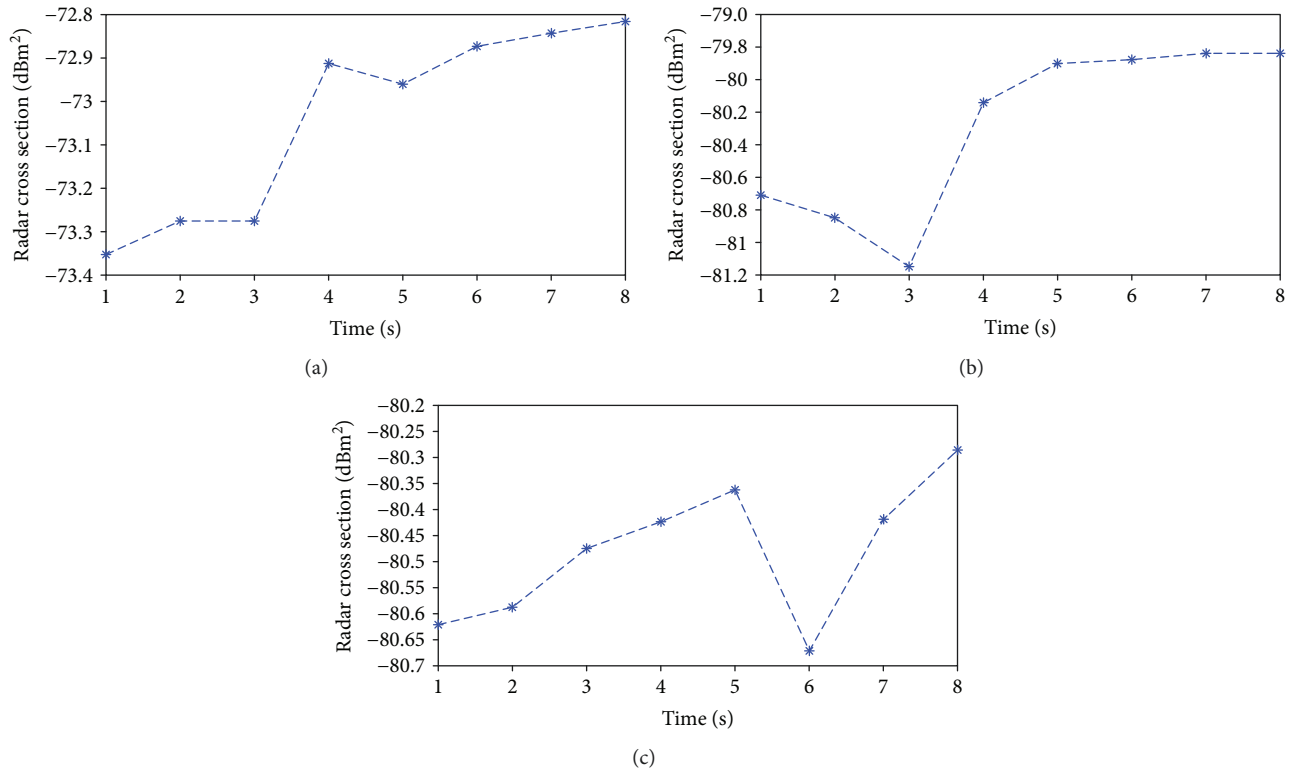

Figure 7: Coherent cumulative averaging results of (a) horizontally rotated hexagonal column particles, (b) horizontally rotated ellipsoidal particles, and (c) horizontally rotated spherical particles by means of MIMO.

respectively, by means of MIMO. In order to study the RCS fluctuation values at different detection methods, we introduced the maximum RCS fluctuation values under each transmission and reception combination of MIMO, which can be found in Table 3.

Table 3 shows that the maximum RCS fluctuation value occurs at the combination of the transmitting antenna 4 and receiving antenna 1 (24.55 dB) for horizontally orientated hexagonal columns; for horizontally orientated ellipsoids, the maximum RCS fluctuation value occurs at the

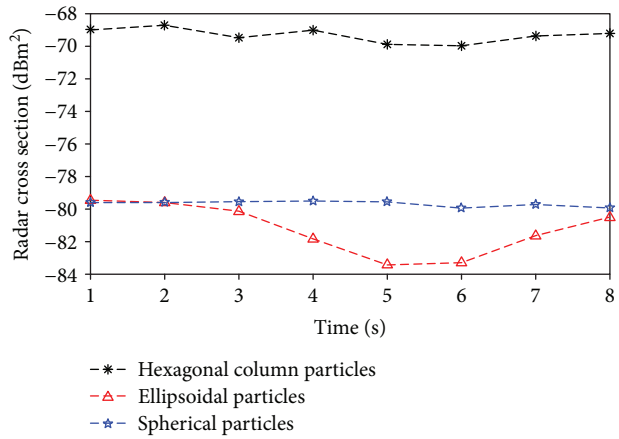

Figure 8: RCS fluctuations of three particles detected by vertically pointing single radar.

Figure 9: MIMO radar testing system.

combination of the transmitting antenna 4 and receiving antenna 1 (32.32 dB); for horizontally orientated spheres, the maximum RCS fluctuation value occurs at the combination of the transmitting antenna 4 and receiving antenna 1 (28.92 dB). The coherent cumulative averaging means that the backscattering signals of all particles have the same phases and we can directly add these signals and then average this added signals; the concrete results of the horizontally orientated hexagonal columns, ellipsoids, and spheres in Figure 6 can be found in Figure 7.

Figure 7 shows that the maximum RCS fluctuations are 0.5374 dB, 1.3126 dB, and 0.3856 dB after the coherent cumulative average processing for horizontally rotated hexagonal column particles, ellipsoidal particles, and spherical particles, respectively. The simulation results of ensembles of particles in Figure 5 vertically detected by single radar (the polarization direction of the electric field along the x-axis and the propagation direction of the electromagnetic wave along the z-axis) can be found in Figure 8.

Figure 8 shows that the maximum RCS fluctuation values of the horizontally rotated hexagonal column particles, ellipsoidal particles, and spherical particles are 1.2668 dB, 3.9765 dB, and 0.4342 dB, respectively. Comparing the results of Figure 7 with those of Figure 8, the coherent accumulation averaging results of horizontally rotated hexagonal column particles, ellipsoidal particles, and spherical particles are smaller than those of the vertically pointing single radar. Therefore, MIMO radar can reduce the RCS fluctuation of the moving particles. The following experiment was used to verify the ability of MIMO radar to suppress echo fluctuation.

4.2. Experimental Measurements of Echo Fluctuation Suppression. The echo fluctuation suppression of moving particles by MIMO at 10 GHz using the PNA vector network analyzer (model: E8363C, test frequency: 10 MHz–40 GHz) from Agilent Technologies, USA, can be transformed into results at 94 GHz by electromagnetic similarity theory [31]. A set of MIMO echo fluctuation suppression systems based on a vector network analyzer in the microwave anechoic chamber of Nanjing University of Information Science and Technology can be found in Figure 9.

The vector network analyzer in Figure 9 has a two-port device, which cannot achieve multi-input and multioutput characteristics of MIMO radar at the same time; however, the time-based transmitting mode of MIMO spatial diversity can be achieved by the different combinations of transmitting ports and receiving ports at different times. The moving particles are divided into eight different states (8-second motion states), and the ensembles of particles consist of 19 cuboid candles (length and width are 23 mm, height is 49 mm, and the dielectric constant is 2.1); we should notice that the cuboid candles have a different dielectric constant as compared to ice.

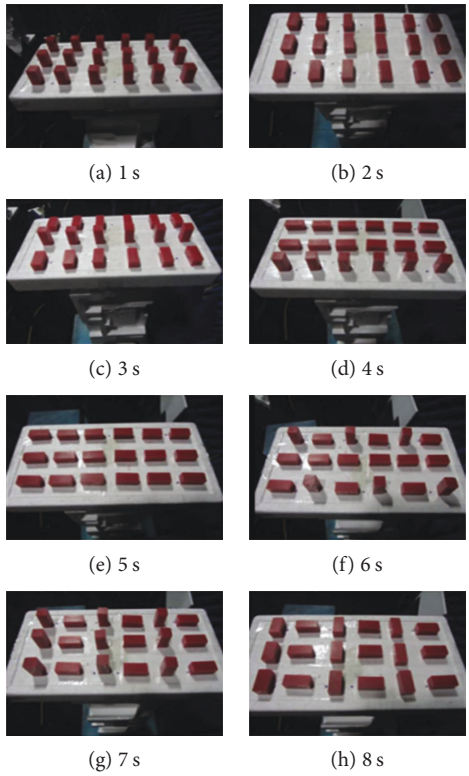

Figure 10: Eight different states of cuboid candles corresponding to different times.

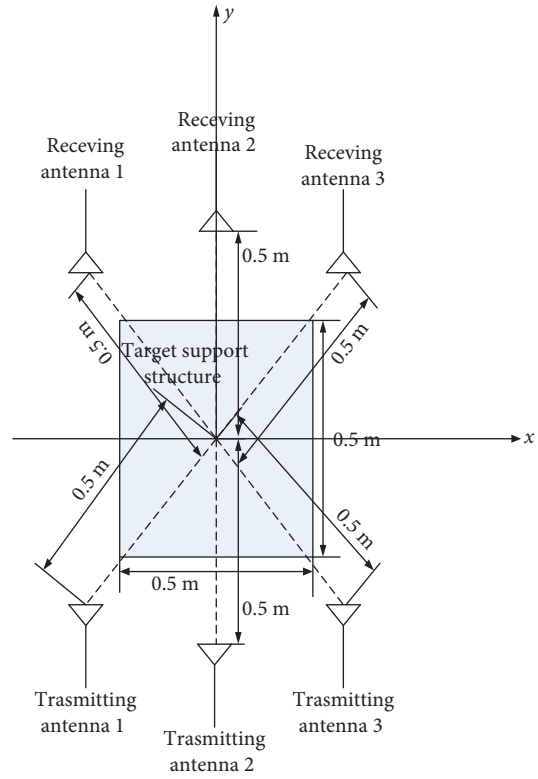

Figure 11: Overhead view of the MIMO antenna positions.

Eight different states of cuboid candles corresponding to different times can be found in Figure 10.

The space to the left and right of the cuboid candles in Figure 10 is 7.5 cm, and the distance between the upper and lower center is 8 cm. The transmitting and receiving positions of the MIMO antenna are shown in Figure 11.

Figure 11 shows the positions of the 3 ∗ 3 MIMO antenna array, and the distances between the transmitting antenna and the center of the target support structure, the receiving antenna, and the center of the target support structure are all 0.5 m. The bottom of the target support structure is a rectangular box with a wave-absorbing characteristic (both the length and width are 0.5 m, and the height is 0.3 m). The overall height of the target support structure is 2.5 m. The horn antenna is placed on a 0.15 m thick foam pad, and the elevation angle of all horn antennas is 78°. The specific positions of the transmitting horns and receiving horns in the MIMO testing experiment can be found in Figure 12.

The location parameters of the transmitting and receiving horns of the 3 ∗ 3 MIMO antenna array in the spherical coordinate system in Figure 12 are shown in Table 4.

The S21 values of the cuboid candles in Figure 10 are detected by the MIMO antenna array in Figure 12 and can be found in Figure 13.

Figure 13 showed the S21 values of moving cuboid candles within 8 s using the vector network analyzer at Nanjing University of Information Science and Technology; these values will be used to compute the RCS values of cuboid candles.

An aluminum plate with dimensions of 50 cm ∗ 50 cm and a thickness of 1.35 mm was used as a calibrator when conducting the MIMO testing experiment. The testing environment can be seen in Figure 14.

The bistatic RCS results of the calibration plate in Figure 14 simulated by HFSS software are shown in Figure 15.

According to the RCS transformation formula [30] and the results of Figures 13 and 15, the RCS fluctuation of the cuboid candles in 8 states can be found in Figure 16.

Figure 16 shows the MIMO detection results of cuboid candles. In order to study the RCS fluctuation values of cuboid candles at different detection methods, we introduced the maximum RCS fluctuation detected by each combination of the MIMO transmitting and receiving antennas, which can be shown in Table 5.

Table 5 shows that the RCS fluctuation is the largest (28.96 dB) for cuboid candles in the combination of transmitting antenna 2 and receiving antenna 2. The results in Figure 16 also showed that RCS fluctuation in the combination of transmitting antenna 2 and receiving antenna 2 is higher than those of other combinations of transmitting antenna and receiving antenna.

The coherent cumulative averaging results of cuboid candles detected by MIMO radar in Figure 16 can be found in Figure 17.

The maximum RCS fluctuation of cuboid candles is 21.24 dB by the coherent cumulative average process, which can be computed in Figure 17. Compared with the maximum RCS fluctuation (transmitting antenna 2, receiving

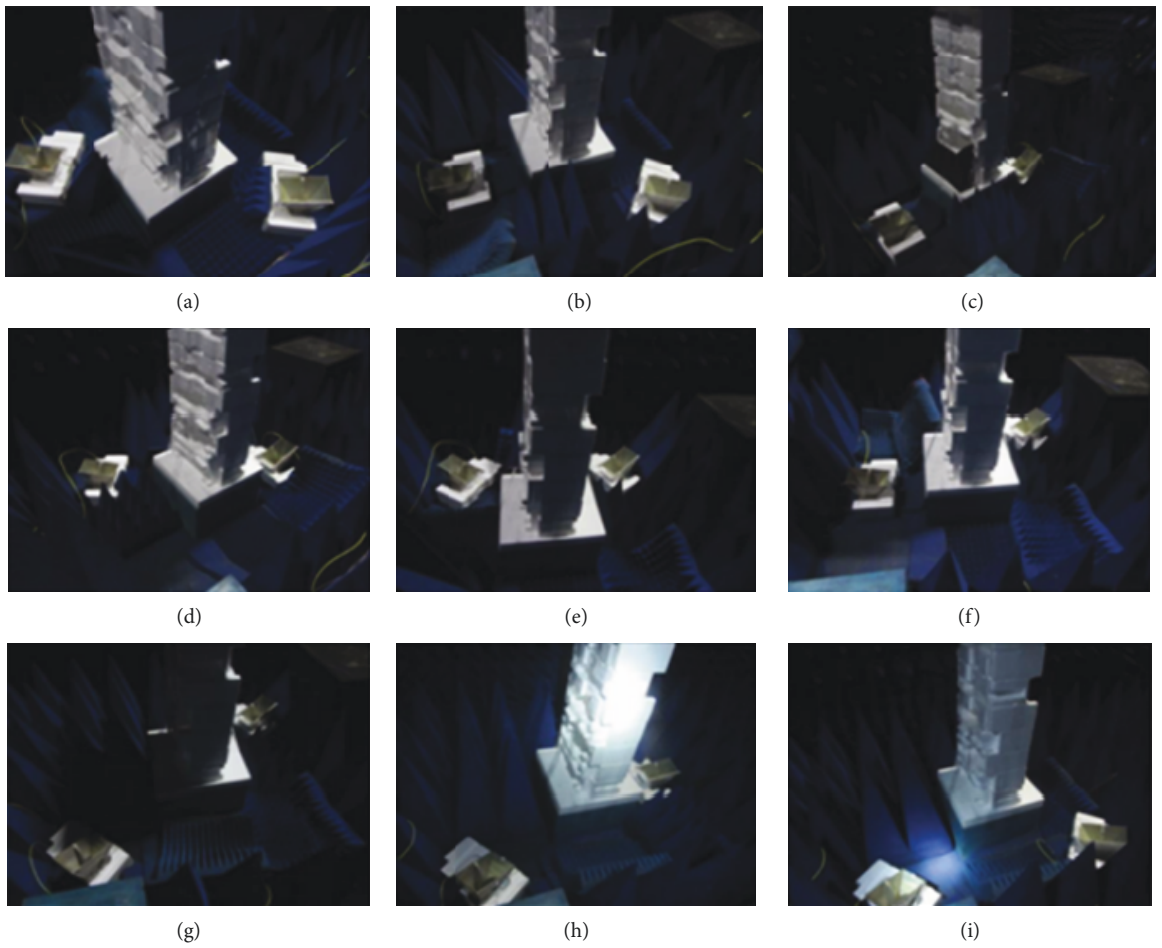

Figure 12: The layout of (a) T1 + R3, (b) T2 + R3, (c) T2 + R2, (d) T1 + R2, (e) T1 + R1, (f) T2 + R1, (g) T3 + R1, (h) T3 + R2, and (i) T3 + R3 of the 3 ∗ 3 MIMO antenna array (T stands for transmitting antenna, R stands for receiving antenna, and + stands for combination).

Table 4: Location parameters of transmitting antennas and receiving antennas in the spherical coordinate system.

Number	Azimuth angle	Pitch angle
T1	225°	168°
T2	270°	168°
T3	315°	168°
R1	135°	168°
R2	90°	168°
R3	45°	168°

T stands for transmitting antenna; R stands for receiving antenna.

antenna 2) in Figure 16, RCS fluctuation has been effectively suppressed.

5. Conclusions

The echo (RCS) fluctuation phenomenon of the moving spherical particles is calculated by using the vector potential method under the Rayleigh approximation. The RCS fluctuation can be suppressed by the video integrator of single millimeter radar, but the average time is very important to

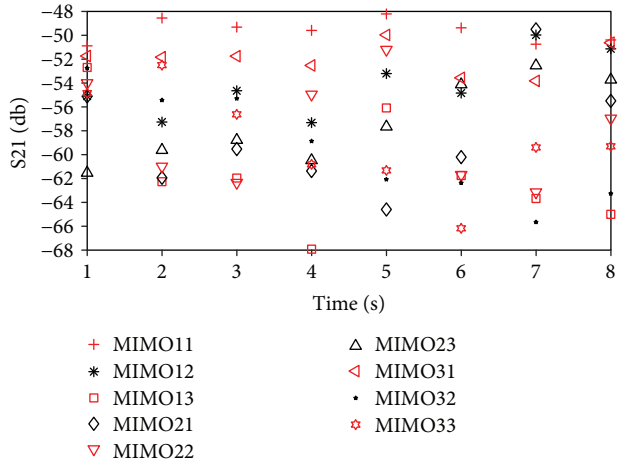

Figure 13: S21 values of moving cuboid candles within 8 s by means of MIMO array.

the suppression effect, which can not only easily lose changed information but also reduce the distance resolution. In addition, a video integrator would reduce the resolution of the

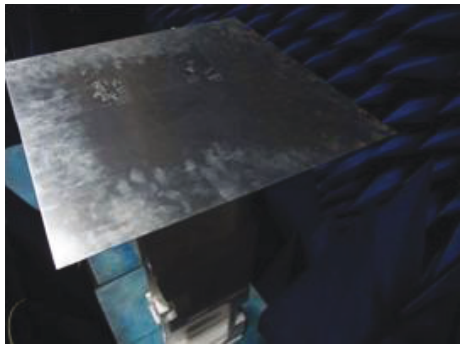

Figure 14: The calibrator for testing the cuboid candles by means of the MIMO array.

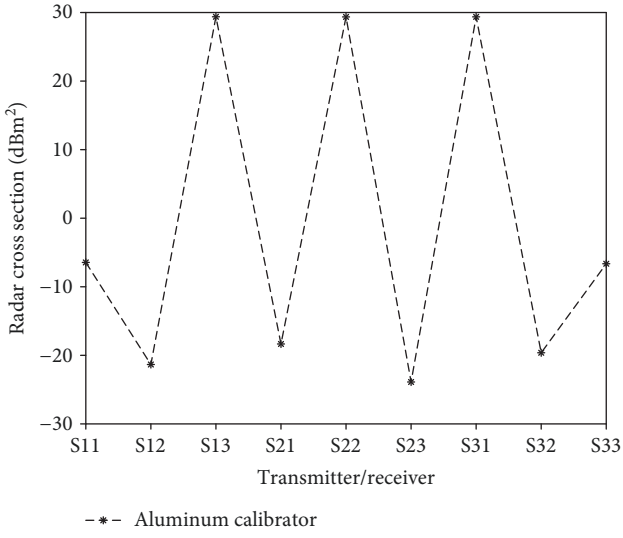

Figure 15: Simulated bistatic RCS values of the 50 ∗ 50 aluminum calibrator.

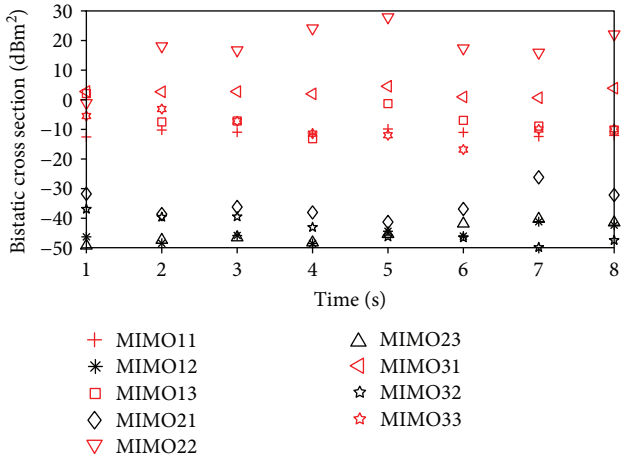

Figure 16: Retrieved RCS values of cuboid candles by means of MIMO.

Table 5: The difference between the maximum and minimum values of RCS fluctuation by means of MIMO (units: dB).

Number	Maximum RCS fluctuation of cuboid candles
T1 + R1	2.67
T1 + R2	7.34
T1 + R3	15.23
T2 + R1	15.10
T2 + R2	28.96
T2 + R3	9.00
T3 + R1	3.85
T3 + R2	12.92
T3 + R3	13.68

T stands for transmitting antenna, R stands for receiving antenna, and + stands for combination.

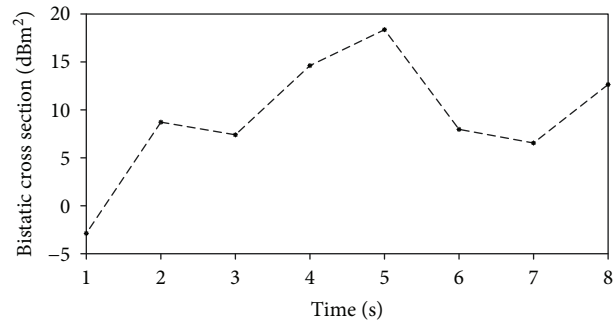

Figure 17: Coherent cumulative averaging values of cuboid candles by means of MIMO array.

radar range. To solve these problems, the RCS values of horizontally orientated hexagonal columns, ellipsoids, and spherical particles were simulated by HFSS software. Compared with the results of detecting moving particles with vertically pointing radar, RCS fluctuation can be effectively reduced by MIMO radar after conducting coherent accumulative averaging processes for the above results. To experimentally validate the RCS fluctuation suppression ability of MIMO radar, RCS values of cuboid candles based on the time-based transmitting mode of MIMO spatial diversity have been measured in a microwave anechoic chamber at Nanjing University of Information Science and Technology; the results showed that the RCS fluctuation of moving particles can be effectively reduced by MIMO radar.

Data Availability

The dataset generated during this study is available from the corresponding author on reasonable request.

Disclosure

The abstract of this paper has been published in *Sixteenth Conference on Electromagnetic & Light Scattering*.

Conflicts of Interest

The authors declare that they have no conflicts of interest.

Acknowledgments

This work was supported by open funding by the Natural Science Foundation of Jiangsu Province (Program no. BK20170945), the Key Laboratory for Aerosol-Cloud-Precipitation of CMA-NUIST (Program no. KDW1703), the National Natural Science Foundation of China (Program nos. 41275004, 61372066, and 41571348), the Startup Foundation for Introducing Talent of Nanjing University of Information Science and Technology (Program no. 2016r028), Earth Science Virtual Simulation Experiment Teaching Course Construction Project of Nanjing University of Information Science and Technology (Program no. XNFZ2017C02), Program for Postgraduates Research and Innovation in Universities of Jiangsu Province under Grant no. SJCX18_0322.

References

[1] K. N. Liou, "Influence of cirrus clouds on weather and climate processes: a global perspective," *Monthly Weather Review*, vol. 114, no. 6, pp. 1167–1199, 1986.

[2] G. L. Stephens, S. C. Tsay, P. W. Stackhouse Jr., and P. J. Flatau, "The relevance of the microphysical and radiative properties of cirrus clouds to climate and climatic feedback," *Journal of the Atmospheric Sciences*, vol. 47, no. 14, pp. 1742–1754, 1990.

[3] D. K. Lynch, K. Sassen, D. O. Starr, and G. Stephens, *Cirrus*, Oxford University Press, New York, NY, USA, 2002.

[4] C. Liu, P. Yang, P. Minnis et al., "A two-habit model for the microphysical and optical properties of ice clouds," *Atmospheric Chemistry and Physics*, vol. 14, no. 24, pp. 13719–13737, 2014.

[5] C. Liu, R. L. Panetta, and P. Yang, "The effects of surface roughness on the scattering properties of hexagonal columns with sizes from the Rayleigh to the geometric optics regimes," *Journal of Quantitative Spectroscopy and Radiative Transfer*, vol. 129, pp. 169–185, 2013.

[6] C. Kummerow, W. Barnes, T. Kozu, J. Shiue, and J. Simpson, "The tropical rainfall measuring mission (TRMM) sensor package," *Journal of Atmospheric and Oceanic Technology*, vol. 15, no. 3, pp. 809–817, 1998.

[7] G. L. Stephens, D. G. Vane, R. J. Boain et al., "The CloudSat mission and the A-Train: a new dimension of space-based observations of clouds and precipitation," *Bulletin of the American Meteorological Society*, vol. 83, no. 12, pp. 1771–1790, 2002.

[8] N. I. Fox and A. J. Illingworth, "The retrieval of stratocumulus cloud properties by ground-based cloud radar," *Journal of Applied Meteorology*, vol. 36, no. 5, pp. 485–492, 1997.

[9] L. Li, S. M. Sekelsky, S. C. Reising et al., "Retrieval of atmospheric attenuation using combined ground-based and airborne 95-GHz cloud radar measurements," *Journal of Atmospheric and Oceanic Technology*, vol. 18, no. 8, pp. 1345–1353, 2001.

[10] K. P. Moran, B. E. Martner, M. J. Post, R. A. Kropfli, D. C. Welsh, and K. B. Widener, "An unattended cloud-profiling radar for use in climate research," *Bulletin of the American Meteorological Society*, vol. 79, no. 3, pp. 443–455, 1998.

[11] S. M. Sekelsky, L. Li, G. A. Sadowy et al., "Measurements of atmospheric extinction using combined airborne and ground-based 95 GHz radar observations," in *IEEE 1999 International Geoscience and Remote Sensing Symposium. IGARSS'99 (Cat. No.99CH36293)*, pp. 461–463, Hamburg, Germany, 1999.

[12] K. Aydin and C. Tang, "Relationships between IWC and polarimetric radar measurands at 94 and 220 GHz for hexagonal columns and plates," *Journal of Atmospheric and Oceanic Technology*, vol. 14, no. 5, pp. 1055–1063, 1997.

[13] M. I. Mishchenko and L. D. Travis, "Capabilities and limitations of a current FORTRAN implementation of the T-matrix method for randomly oriented, rotationally symmetric scatterers," *Journal of Quantitative Spectroscopy and Radiative Transfer*, vol. 60, no. 3, pp. 309–324, 1998.

[14] P. Yang and K. N. Liou, "Finite-difference time domain method for light scattering by small ice crystals in three-dimensional space," *Journal of the Optical Society of America A*, vol. 13, no. 10, pp. 2072–2085, 1996.

[15] B. T. Draine and P. J. Flatau, "Discrete-dipole approximation for scattering calculations," *Journal of the Optical Society of America A*, vol. 11, no. 4, pp. 1491–1499, 1994.

[16] M. Morgan and K. Mei, "Finite-element computation of scattering by inhomogeneous penetrable bodies of revolution," *IEEE Transactions on Antennas and Propagation*, vol. 27, no. 2, pp. 202–214, 1979.

[17] R. F. Harrington, *Field Computation by Moment Methods*, Macmillan Press, New York, NY, USA, 1968.

[18] T. L. Schneider and G. L. Stephens, "Theoretical aspects of modeling backscattering by cirrus ice particles at millimeter wavelengths," *Journal of the Atmospheric Sciences*, vol. 52, no. 23, pp. 4367–4385, 1995.

[19] P. C. Zhang, B. Y. Du, and T. P. Dai, *Radar Meteorology*, Meteorology Press, Beijing, China, 2000.

[20] L. G. Yuan and P. He, "Video integrator and processor of weather radar," *Journal of Guangxi Meteorology*, vol. 9, no. 4, pp. 72–76, 1988.

[21] J. S. Marshall and W. Hitschfeld, "Interpretation of the fluctuating echo from randomly distributed scatterers. Part I," *Canadian Journal of Physics*, vol. 31, no. 6, pp. 962–994, 1953.

[22] G. Mie, "Beiträge zur optik trüber medien, speziell kolloidaler metallösungen," *Annalen der Physik*, vol. 330, no. 3, pp. 377–445, 1908.

[23] N. A. Logan, "Survey of some early studies of the scattering of plane waves by a sphere," *Proceedings of the IEEE*, vol. 53, no. 8, pp. 773–785, 1965.

[24] S. J. Zhang, *Theory of Electromagnetic Engineering*, Sciences Press, Beijing, China, 2009.

[25] L. Rayleigh, "On the light from the sky, its polarization and colour," *Philosophical Magazine*, vol. 41, pp. 107–120, 1871.

[26] H. C. Van de Hulst, *Light Scattering by Small Particles*, Dover Press, Mineola, NY, USA, 1981.

[27] C. F. Bohren and D. R. Huffman, *Absorption and Scattering of Light by Small Particles*, Wiley Press, Hoboken, NJ, USA, 1983.

[28] K. F. Evans and G. L. Stephens, "Microwave radiative transfer through clouds composed of realistically shaped ice crystals. Part I. Single scattering properties," *Journal of the Atmospheric Sciences*, vol. 52, no. 11, pp. 2041–2057, 1995.

[29] Z. Zhang, P. Yang, G. W. Kattawar et al., "Geometrical-optics solution to light scattering by droxtal ice crystals," *Applied Optics*, vol. 43, no. 12, pp. 2490–2499, 2004.

[30] K. F. Evans and G. L. Stephens, "Microwave radiative transfer through clouds composed of realistically shaped ice crystals. Part II. Remote sensing of ice clouds," *Journal of the Atmospheric Sciences*, vol. 52, no. 11, pp. 2058–2072, 1995.

[31] J. Wang, J. Ge, Q. Zhang et al., "Radar cross-section measurements of ice particles using vector network analyzer," *AIP Advances*, vol. 6, no. 9, article 095310, 2016.